Microphotoluminescence studies of single quantum dots. I. Time-resolved experiments

U. Bockelmann and W. Heller
Walter Schottky Institut, Technische Universität München, Am Coulombwall, 85748 Garching, Germany

A. Filoramo and Ph. Roussignol
Laboratoire de Physique de la Matière Condensée, Ecole Normale Supérieure, 24 rue Lhomond, 75005 Paris, France

(Received 13 May 1996)

Photoluminescence measurements with combined spatial, temporal, and spectral resolution are performed on single GaAs/$Ga_xAl_{1-x}As$ quantum dots. The complete spatial quantization leads to a spectrum of discrete emission lines. A series of structures with various confinement strength is investigated, as a function of excitation wavelength, excitation power, and temperature. In all cases, a fast rise of the luminescence is observed. Several independent results show that Coulomb scattering plays a major role within the early stage of energy relaxation. At liquid-helium temperature, a strikingly different recombination dynamics is observed for dots with various lateral potential. For weak lateral confinement, energy relaxation is directly observed in the time dependence of the luminescence spectrum. In contrast, in the sample with strongest confinement, independent recombination of the discrete lines occurs. Increasing the excitation power, higher-energy lines appear and the spectral weight shifts systematically from the lowest to the higher-energy lines. For this variation, which corresponds to an increase in the estimated number of electron-hole pairs in the single dot from about 1–2 to 200, the peak energies hardly change. We have also performed detailed calculations of the energy spectrum and the relaxation and recombination times of excitons in quantum dots. The experimental results are surprisingly well interpreted assuming the formation of an exciton gas obeying the Pauli exclusion principle. [S0163-1829(97)06907-5]

I. INTRODUCTION

The charge carriers in quantum dots are confined in all three spatial directions. In analogy to the case of atoms or molecules this leads to a discrete energy spectrum. The conduction-band states of semiconductor quantum dots have been studied experimentally by intraband absorption of infrared light,[1,2] resonant tunneling,[3–5] capacitance spectroscopy,[2,6,7] and Raman scattering.[8] In intraband absorption, dipole transitions between the n-electron ground state and n-electron excited states are probed. For nearly parabolic lateral confinement potentials, usual for samples with a lateral confinement induced by structured gates, the transition energies are insensitive to many-body effects. The dipole operator only couples to excited states of the center-of-mass coordinate without affecting the relative motion of the individual carriers. This result is usually called the generalized Kohn theorem.[9,10] Electron transport through quantum dots, such as resonant tunneling and capacitance spectroscopy, is strongly influenced by charging effects. The Coulomb blockade is an interesting phenomenon in itself but hampers the determination of the intrinsic electron spectrum. Raman scattering is a powerful technique that allows one to measure the energy splitting between the n-electron ground state and excited states in quantum dots. For small n, the method is very difficult for intensity reasons, but on the other hand there are no limitations due to the generalized Kohn theorem or charging effects.

Photoluminescence (PL) spectroscopy is the most widely used optical characterization tool for semiconductor quantum dots. The PL properties are of central importance for optical applications as light detectors, emitters, modulators, or lasers. In contrast to the measurement techniques described above, PL spectroscopy probes not only the conduction band but transitions between valence- and conduction-band states. The PL spectrum contains a number of important informations that are sometimes difficult to extract. It reflects the conduction- and valence-band structure, the dynamics of relaxation and recombination, and is sensitive to excitonic and many-body effects.

Although fabrication techniques for artificial semiconductor structures have been greatly improved, inhomogeneities still remain within arrays of one-dimensional (1D) or 0D structures. Up to now, most experimental studies have been performed on such arrays exhibiting fluctuations of size and/or composition. In optical spectroscopy, this leads to inhomogeneous broadening, which hampers the study of the intrinsic properties of the low-dimensional system.[11,12]

Space-resolved spectroscopy allows the investigation of an individual quantum structure. The PL spectrum of a single quantum dot should not be affected by inhomogeneous broadening. Local potential fluctuations in a single dot may modify the quantization energy of discrete atomiclike levels, but should not cause line broadening.

In the microphotoluminescence (μ-PL) experiment, local excitation and detection are achieved with a resolution of about 1 μm by the use of an optical microscope objective. With μ-PL it has been shown on specially designed single quantum dot structures, that the discrete radiative transitions between 0D states can be measured in semiconductor heterostructures.[12,13] The μ-PL spectrum of a single dot consists of sharp, atomiclike lines, in contrast to the broad spectra observed by ordinary PL spectroscopy on arrays of quantum dots. The μ-PL technique is versatile and powerful. The

spatial resolution of excitation and detection can be varied independently and the efficient collection allows spectroscopy with very weak excitation. The excitation conditions are well characterized, the dependences on the wavelength, intensity, and polarization of the exciting beam provide detailed information on the intrinsic optical properties of a nanostructure. Narrow, 0D-like transitions can be observed by μ-PL also on single quantum wells.[14–17] These lines are attributed to excitons confined to a local interface imperfection. As an example of the power of the technique, even confined biexcitons could be identified by a quadratic dependence on the excitation power, a distinct polarization dependence and a two-photon absorption line in the μ-PL excitation spectrum.[16] The sharp lines related to interface imperfections in quantum wells have been observed also by near-field scanning optical microscopy (NSOM).[18] With NSOM a better spatial resolution can be obtained to the expense of sensitivity. For the example of a spatial resolution of 100 nm in the visible spectral range, about three orders of magnitude of the signal are lost in this nonimaging technique.[19,20] To our knowledge, NSOM spectroscopy with local detection could not yet be performed under reasonably low excitation conditions. Finally, cathodoluminescence has also been employed successfully to avoid inhomogeneous broadening by spectroscopy of single quantum dots.[21] In this case, local excitation is provided with high excess energy and the spatial resolution is limited by the diffusion length of the electrically injected carriers.

In the present two papers, we report on a detailed investigation of the optical properties of single quantum dots. The samples have been fabricated by laser-induced local interdiffusion of a GaAs/$Ga_xAl_{1-x}As$ quantum-well heterostructure. We have realized a μ-PL experiment with picosecond time resolution, which allows us to follow the line spectrum of a single dot directly in the time domain.[22,23] This paper (part I) contains a comprehensive discussion of these time-resolved studies. In the following paper [part II (Ref. 24)], results of another experiment are presented: μ-PL spectroscopy of the single quantum dots in high magnetic field.

With the time-resolved measurements, we address a number of important open questions regarding the dynamics of relaxation and recombination in quantum dots. It has been predicted theoretically that phonon-assisted relaxation should be considerably slowed down by complete spatial quantization.[25–27] In typical quantum dot structures, the relaxation by LA phonon scattering should be efficient only between levels with an energy separation smaller than a few meV. LO phonon emission (and two phonon LO+LA mechanisms) is possible only for energy separations within a few meV from a LO branch. Relaxation by Coulomb scattering via an Auger-like process has also been considered.[28] This relaxation mechanism is expected to be efficient in the presence of a dense electron-hole plasma, even for small dots where the phonon scattering rates are low. In addition to the information on the energy relaxation properties, our time-resolved studies also provide new and unexpected insight into the spectrum and the recombination dynamics of an interacting electron-hole plasma in a quantum dot.

This paper is organized as follows. In Sec. II, we describe the investigated series of single quantum dot structures. In Sec. III, we briefly discuss some of the basic physical concepts underlying the time-resolved PL of quantum dots. Section IV contains a description of the experimental setup. The presentation of the experimental results in Sec. V is divided into four parts according to the different parameters that have been systematically varied: the excitation wavelength (A), the excitation power (B), the lateral confinement (C), and the sample temperature (D). A concluding discussion is given in Sec. VI.

II. SAMPLES

Both the time-resolved and the magnetic-field experiments are performed on single quantum dot structures fabricated by laser-induced local interdiffusion. This section gives a brief description of the fabrication process, while more detailed accounts have been published elsewhere.[12,29] The samples have been characterized in detail by cw μ-PL spectroscopy.[12,30]

A schematic cross section of a dot structure is given in the inset of Fig. 1 of Ref. 12. The starting material is a 3-nm-wide, undoped GaAs/$Ga_{0.65}Al_{0.35}As$ single quantum well grown by molecular beam epitaxy. A band-gap modulation is produced by locally heating the sample by an Ar^+ laser beam focused to a spot of about 500 nm full width at half maximum (FWHM). An external laser power stabilizer and an autofocus system are used to keep the laser intensity on the sample surface constant. Thermal interdiffusion of the well and barrier layers takes place underneath the spot center. A dot structure is defined by first drawing a square frame of size w with the focused laser beam. Subsequently an area of 6×6 μm around the dot is interdiffused by scanning the beam continuously. This procedure gives rise to a lateral modulation of the band gap as shown schematically in the lower part of the inset. The strongly nonlinear temperature dependence of the interdiffusion allows one to realize steep lateral barriers for electrons and holes.

In Fig. 1 of Ref. 12 and Fig. 4 of Ref. 30, μ-PL spectra collected on different quantum dots at liquid-helium temperature are presented. Only one dot is measured at a time and consequently there should be no inhomogeneous broadening of the spectra. Indeed, the PL lines of the quantum dots are much smaller than the inhomogeneously broadened line of the as-grown quantum well (7 meV FWHM). The energy shift of the lowest PL line is a combined effect of lateral confinement and alloying of the dot center. The effective size of the lateral confinement is given by the interdiffusion profile and not just by the geometrical size w. This can be seen in Fig. 6 of Ref. 29, where the effective lateral modulation of the band edges, theoretically expected for structures with $w=600$, 450, and 300 nm, is presented. Decreasing w from large values, the laser-induced barriers move closer together, which leads to an increasing lateral quantization. Maximum confinement is obtained when the barriers are about to meet at the dot center. We expect this to be realized in the $w=450$ nm dot where a maximum line splitting of about 10 meV is observed. Decreasing w further, the increasing Al content near the center of the dot leads to a strong blueshift of the PL ground state, but a decreasing lateral barrier height. For $w\rightarrow 0$, we approach the case of a homogeneously alloyed 2D layer without lateral confinement. Section III A 2 contains a comparison of the experimental PL spectra with

calculated exciton states. It is important to remember that the correct measure for the strength of the lateral confinement is the line splitting of the μ-PL spectrum and not the geometrical size w.

III. BASIC CONCEPTS

In this section we discuss some of the basic concepts relevant to the time-resolved PL of quantum dots. It is divided into three parts: (A) the eigenstates of the electronic system, (B) the mechanisms of energy relaxation after optical excitation, and (C) the theoretically expected properties of an exciton gas in a quantum dot.

A. Electron-hole pairs in quantum dots

1. Independent electron-hole pair

The simplest way to describe the luminescence spectrum is to consider band-to-band transitions between single-particle states. The lateral potential and the lowest heavy-hole and electron states, calculated for our laser fabricated dots, are presented in Fig. 6 of Ref. 29. In these samples, the confinement is much stronger in the growth direction than in the lateral directions. Therefore it is a good approximation for the near-band-edge states to consider the lateral motion as independent and to neglect valence-band mixing. In the general case, there is a coupling between the different spatial directions and each valence-band state is a mixture of heavy- and light-hole components. A calculation of hole levels in quantum dots including valence-band mixing can be found in Refs. 31 and 32.

Already the single-particle spectrum is discrete in quantum dots. Therefore the electron hole Coulomb attraction does not have the same qualitative effect as in systems of higher dimensionality where it introduces discrete transitions in an originally continuous spectrum. In small dots, where the confinement energy strongly exceeds the energy associated with the Coulomb attraction, the independent electron-hole pair picture is adequate. This situation can be realized, for example, in epitaxially grown strained semiconductor island structures.[13,21,33,34] In the corresponding calculations the electron hole Coulomb attraction can be treated as a weak perturbation.[35]

2. Single exciton

When the spatial confinement is comparable to or weaker than the Coulomb attraction, the single-particle levels are strongly mixed and the independent electron-hole pair picture breaks down. This is the case in our samples. The reader may compare the level splittings in Fig. 1 of Ref. 12 with the exciton binding of a GaAs quantum well (of the order of 10 meV). In principle, the exciton concept applies only to the case of one electron-hole pair in the dot. Experimentally this means a low excitation power, which ensures that the average number of pairs is less than one. The cw spectra presented in Ref. 12 and 30 correspond to this single exciton regime. The estimation derived in Sec. V B gives a value of 10^{-2} pairs in time-average for the 125-nW spectra of Fig. 4 of Ref. 12. The measured magnetic field shifts of the μ-PL lines presented in part II (Ref. 24) also show the excitonic character of the single quantum dot spectra.

Theoretical results for the energy spectrum and radiative lifetimes of quantum dot excitons are presented in Fig. 3 of Ref. 22. We consider the effective-mass Hamiltonian

$$H = H_0 + H_{eh},$$

$$H_0 = \sum_{\nu=e,h} \frac{-\hbar^2}{2m_\nu}\left(\frac{\partial^2}{\partial x_\nu^2} + \frac{\partial^2}{\partial y_\nu^2}\right) + \frac{1}{2} m_\nu \omega_\nu^2 (x_\nu^2 + y_\nu^2),$$

$$H_{eh} = -\int dz_e \int dz_h |\chi_e(z_e)|^2 |\chi_h(z_h)|^2 \frac{e^2}{\epsilon_l |\mathbf{r}_e - \mathbf{r}_h|}. \quad (1)$$

H_{eh} describes the electron-hole Coulomb attraction screened by the static dielectric constant ϵ_l and weighed over the ground subband wave functions χ_e, χ_h of the quantum well. The lateral confinement, included in H_0, is described by parabolic potentials with rotational symmetry in the xy plane. We use $\omega_h = \omega_e (m_e/m_h)^{1/2}$ so that the electron and hole parabola have the same curvature, as suggested by the calculated band edge profiles presented in Fig. 6 of Ref. 29 for $w = 450$ nm. Thus, a single parameter, the energy $\hbar\omega_e$, describes the strength of the lateral confinement in this model. The Hamiltonian H is diagonalized numerically by an expansion on the analytical eigenfunctions of H_0. The latter are parametrized by the radial quantum numbers n_e, n_h and the angular momentum quantum numbers l_e, l_h of the 2D harmonic oscillator. The invariance of H to rotations around the z axis implies the conservation of the total angular momentum $j = l_e + l_h$ of the exciton envelope function. Only excitons with $j = 0$ decay radiatively, while the other states are not coupled to the light in the dipole approximation. The radiative lifetime τ^R of a particular state is obtained from its envelope function $\psi_{ex}(\mathbf{r}_e, \mathbf{r}_h)$ according to[36]

$$\tau^R \propto \left| \int d\mathbf{r} \psi_{\mathrm{ex}}(\mathbf{r}, \mathbf{r}) \right|^{-2}. \quad (2)$$

We first emphasize that the spectrum of radiative states is dominated by a series of almost equidistant lines, with a spacing that increases with $\hbar\omega_e$. Disregarding the mixing of the center of mass and the relative exciton coordinate by the lateral potential, we can approximatively ascribe these main lines to the confinement of the center-of-mass motion in the parabolic potential. Another important point to notice is the strong increase of the density of the nonradiative ($j \neq 0$) levels with increasing energy. This also is a property of the parabolic potential shape. Remember that the degeneracy of the single-particle states of a 2D harmonic oscillator increases linearly with energy.

The cw PL spectra collected on the $w = 400$ and 500 nm dots are dominated by their lowest-energy peak but display clear structures of almost equidistant spacing at higher photon energy. The position of the experimental lines compares quite well with the calculated exciton energies if we consider $\hbar\omega_e = 3$ meV (2 meV) for $w = 400$ nm (500 nm). For the 450-nm dot our model of the local thermal interdiffusion gives $\hbar\omega_e = 6$ meV. The 10-meV splitting between the lowest two peaks agrees with Fig. 3 of Ref. 22, but the threefold splitting of the excited state (Ref. 12, Fig. 4) is not borne out by the calculation. This fine structure cannot be explained either by varying the ratio ω_e/ω_h.[30] However, the first ex-

cited radiative state is almost degenerate with the lowest $j=\pm 2$ state. A deviation of the lateral potential from rotational symmetry would mix the three states; i.e., the nonradiative excitons would gain oscillator strength. Such a deviation can be caused by charged defects introduced by the laser processing in the area surrounding the dot or simply by not perfectly constant interdiffusion conditions during writing the square frame that defines the dot.

3. Interacting electron-hole plasma

The situation becomes increasingly complicated when more than one electron-hole pair is present in the dot. For two pairs, the formation of a biexciton state has been theoretically predicted[37] and experimentally observed.[16] Studying a rather simple model of a quantum dot with only two electron and two hole levels (apart from spin), Barenco and Dupertuis[38] have calculated the spectrum for up to 4 interacting electron-hole pairs. They find very intricate spectra, which sensitively depend on the number of carriers.

The parabolic potentials, which are used to describe our structures, have special properties concerning interaction effects. The generalized Kohn theorem states that for parabolic quantum dots the spectrum of dipole transitions between states from the same parabolic band only reflect single-particle energies.[9,10] This theorem, however, does not apply to interband transitions and we expect to see many-body effects in the luminescence even for parabolic confinement.

B. Mechanisms of energy relaxation

1. Phonon scattering

The most efficient phonon scattering mechanism in the polar III-V compounds is the interaction with LO phonons. Typical scattering rates are of the order of 10^{12}–10^{13} s^{-1}. A first-order phonon emission or absorption process is possible only if the energy separation between the initial and final electron states matches the phonon energy. In quantum dots, the discrete electronic energy spectrum together with the very weak energy dispersion of the LO phonon prevents the Fröhlich interaction in the general case.

On the other hand, scattering by LA phonons is possible over a wide energy range. However, it has been shown theoretically that, although the mechanism remains possible, the rates of electron–LA-phonon scattering in quantum dots decrease drastically when the energy level separation exceeds a threshold E_t.[25] Although momentum conservation is relaxed due to the spatial confinement, above E_t the energy conservation requires scattering by LA phonons with a wave vector too large to be accommodated by the electron. The threshold energy E_t, given by $E_t=\hbar c_s 2\pi/L$, only depends on the sound velocity c_s (3700 m/s for GaAs) and the smallest dimension of the quantum dot L. Throughout our series of quantum dots $E_t=5.1$ meV is constant; the value of $L=3$ nm is given by the width of the underlying quantum well. Due to the larger effective mass the hole level splitting is smaller than the electron one and therefore hole relaxation in quantum dots remains efficient down to somewhat smaller lateral structure size.

The described relaxation bottleneck exists in a similar way also for excitons in quantum dots.[36] In this case, the threshold value E_t has to be compared to the level separations within the exciton energy spectrum. Applied to the calculated spectrum of Fig. 3 of Ref. 22 we notice the following. For $\hbar\omega_e=6$ meV, direct scattering between the main radiative lines is widely suppressed. At high energy efficient relaxation is possible via the closely spaced nonradiative levels, while we expect a rather slow relaxation from the first excited to the ground radiative state. For weaker lateral confinement, $\hbar\omega_e=2$ meV, there should be efficient relaxation directly between the radiative levels all the way down to the ground state (in this case the separation of the radiative levels is smaller than E_t). Experimentally, the most prominent excited-state transitions are observed in the sample where the level splitting is maximum, which is consistent with the slowing down of relaxation with increasing lateral confinement. A detailed description of the theoretical work on the spectrum, relaxation, and radiative recombination of quantum dot excitons are given in Ref. 36, together with calculations on the relative intensity of the PL lines.

2. Coulomb scattering, Auger mechanism

In contrast to the phonon scattering mechanism where the excess energy of the photo-generated carriers is transformed into lattice vibrations, Coulomb scattering between the charge carriers only causes an energy redistribution within the electronic system. Such a redistribution can nevertheless be very important for the thermalization. It allows a large number of carriers to access a few particular efficient relaxation channels. One example is the rapid cooling of an electron gas through emission of LO phonons by electrons in the tail above $\hbar\omega_{\mathrm{LO}}$ of their distribution.

Bockelmann and Egeler have proposed and studied the following, Auger-like mechanism for efficient electron relaxation in quantum dots.[28] In a typical PL experiment electron-hole pairs are excited close to or above the barriers of the lateral potential. Depending on the excitation intensity and the efficiency of relaxation, an electron-hole plasma of sizable density can be present in this energy range. An electron in an excited quantum dot state can now relax by transferring its energy to the plasma by Coulomb interaction in an Auger-like process. A scattering event involves a transition between two quantum dot states and a single-particle (electron or hole) or collective plasma excitation. The plasma itself, placed in an energy region with a quasicontinuous spectrum, can easily thermalize by phonon scattering. For a plasma density of 10^{10} cm^{-2}, the calculated Auger scattering rate of an electron in the first excited dot level exceeds 10^{11} s^{-1}, even for small lateral dot size where relaxation by LA phonon emission is inefficient.[28] In the dot structures investigated here the described Auger mechanism is possible also for resonant excitation within the dot. Here the narrowly spaced higher-energy states play the same role as the 2D continuum states above the lateral potential barrier play in the calculations.

C. Exciton gas

In this section we discuss some properties of a gas of noninteracting excitons in a quantum dot. At first sight it does not seem to make much sense to extend the single exciton picture to a situation with more than one electron-hole

pair in the dot, since as mentioned in Sec. III A 3, few-body interaction effects are expected to have a strong impact on the energy spectrum. The motivation for this discussion is twofold. (i) Our experimental spectra, which will be presented in Sec. V, show a surprisingly weak dependence on the number of excitons in the dot and therefore suggest such an excitonic description. (ii) Even a rough theoretical description may be a helpful guideline since, to our knowledge, no more realistic theoretical description is available, neither for the few-electron-hole pair spectrum nor for the dynamics of relaxation and recombination.

1. Bose or Fermi statistics?

The Wannier exciton is a many-body excited state of the solid. Even if we disregard this aspect in the simple electron-hole picture, we deal with a composite of two half-integer spin particles. In quantum dot samples where the effects of lateral confinement and exciton binding are of similar importance, the average distance between the excitons is never large compared to the exciton radius. Therefore already in the limit of two excitons the composite character is revealed and the Pauli exclusion principle should be important. The latter acts between the two electron and the two hole components. In consequence, there should be no low-density regime corresponding to an exciton gas of Bose statistics in quantum dots. In the limit of small dots, where the spectrum becomes increasingly well described in terms of independent electron-hole pairs we expect to recover the Fermi statistics of the electron and hole. If Fermi statistics is assumed, the curves presented in the left part of Fig. 3 of Ref. 22 give the Fermi energy as a function of the number of excitons N_{ex} at zero temperature. Strictly speaking, as a composite particle the exciton obeys neither a pure Fermi nor a pure Bose statistics, but in the following we nevertheless consider these two limiting cases.

2. Dynamics of relaxation and recombination

In this section we present some theoretical results on the dynamics of an exciton gas in a quantum dot. We study the behavior of exciton gases, where in one case a Fermi and in the other case a Bose statistics is assumed. Qualitatively different results are obtained. For Fermi statistics, Pauli blocking of relaxation can strongly modify the time-resolved optical response. The following set of rate equations is considered:

$$\frac{dn_i}{dt}=\sum_{j\neq i}\tau_{ji}^{-1}n_j(1-\lambda n_i)-n_iS_i. \tag{3}$$

This determines the time dependence of the occupation probability n_i for all quantum dot exciton states. The first term on the right side describes scattering into the state i, the second gives the particle loss out of this state. The parameter λ determines the quantum statistics. $\lambda=0$ stands for Bose-Einstein and $\lambda=1$ for Fermi-Dirac statistics. For $\lambda=1$, the Fermi factors suppress scattering into occupied states and ensure that $n_i\leqslant 1$. At the lattice temperature T_l, the scattering rate between two levels i and j, separated by an energy $\hbar\omega_{ij}=E_i-E_j$, reads

$$\tau_{ij}^{-1}=\tau_{ij}^{0\,-1}[n_P(|\omega_{ij}|,T_l)+\tfrac{1}{2}+\tfrac{1}{2}\mathrm{sgn}(\omega_{ij})]. \tag{4}$$

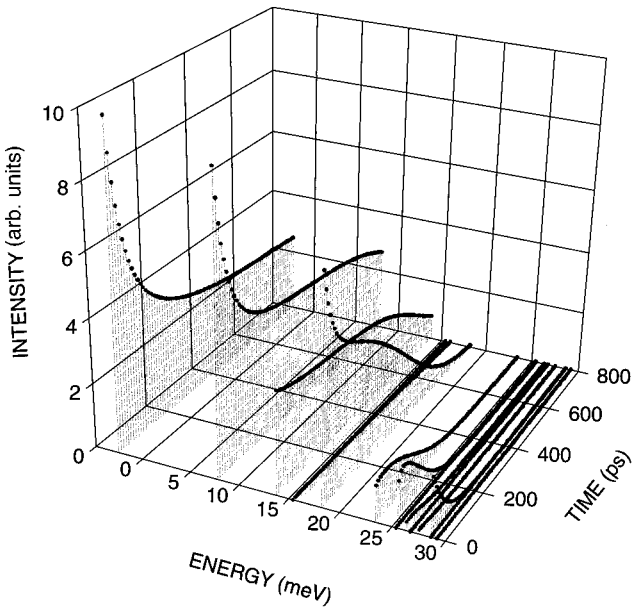

FIG. 1. Calculated PL spectrum as a function of time for an exciton gas in a quantum dot with parabolic lateral potentials of $\hbar\omega_e=6$ meV. At the time origin a Fermi distribution is assumed with $N_{\mathrm{ex}}=50$ excitons and a temperature T_{ex} of 4 meV. The theoretical model includes LA phonon scattering (calculated rates), radiative recombination (calculated), and nonradiative recombination (with a rate P of 2×10^9 s^{-1} for all levels) of the excitons. The Pauli exclusion principle is included in the rate equation. A lattice temperature T_l of 10 K is used.

Between square brackets, the Planck distribution n_P gives the number of phonons present in equilibrium at the lattice temperature T_l. For $\omega_{ij}>0$ this number is increased by one to account for spontaneous phonon emission [$\mathrm{sgn}(x\geqslant 0)=1$, $\mathrm{sgn}(x<0)=-1$]. The scattering times τ_{ij}^0 are calculated to first order of perturbation theory, assuming the deformation potential interaction with one bulk LA phonon.[36,39] For the loss rate

$$S_i=P+\tau_i^{R\,-1}+\sum_{j\neq i}\tau_{ij}^{-1}(1-\lambda n_j) \tag{5}$$

we consider, in addition to LA phonon scattering (last term), nonradiative recombination (described by a single phenomenological rate P for all levels) and radiative recombination [τ_i^R according to Eq. (2)]. From the solution of Eq. (3) we directly obtain the time-dependent luminescence spectrum since the intensity emitted from the exciton state i is given by

$$J_i\propto n_i\tau_i^{R\,-1}. \tag{6}$$

We assume the initial distribution

$$n_i(t=0)=(1+e^{(E_i-\mu)/T_{\mathrm{ex}}})^{-1}.$$

This Fermi distribution is characterized by the temperature T_{ex} and the number of excitons N_{ex}. The chemical potential μ is determined by N_{ex}, T_{ex}, and the calculated energy spectrum. The initial condition is used as a very simple description of the system shortly after an excitation pulse, which is followed by fast carrier relaxation through com-

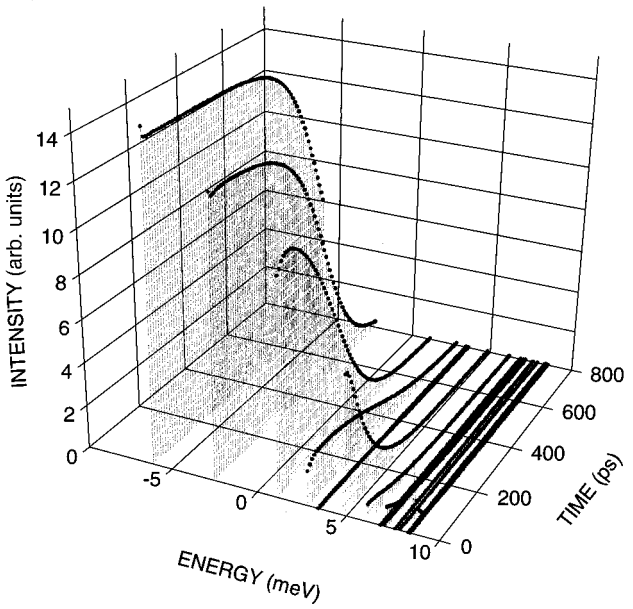

FIG. 2. Same as Fig. 1, for a lateral potential with $\hbar\omega_e = 2$ meV.

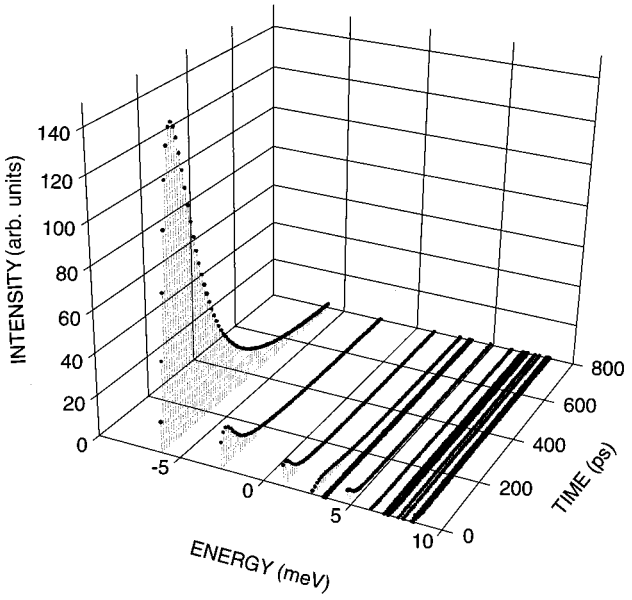

FIG. 4. Same as Fig. 1, for a lateral potential of $\hbar\omega_e = 2$ meV and without Pauli exclusion.

bined LO-phonon and Coulomb scattering. The present rate equation analysis is restricted to the time and energy range where LA phonon scattering represents the dominant mechanism.

The set of scattering times τ_{ij}^0 and radiative lifetimes τ_i^R is calculated for the 100 lowest exciton states, only once for each dot of given $\hbar\omega_e$. This allows a systematic study of the effects of the lattice temperature T_l, the nonradiative loss rate P, the exciton number N_{ex}, the temperature T_{ex}, and the parameter λ, which determines the quantum statistics.

Typical results of a numerical solution of Eq. (3) are presented in Figs. 1–4. The same initial distribution with $N_{\mathrm{ex}} = 50$, $T_{\mathrm{ex}} = 4$ meV is assumed, applied to dots with $\hbar\omega_e = 2$ meV and $\hbar\omega_e = 6$ meV, for both $\lambda = 0$ and $\lambda = 1$. We find qualitatively different dynamics for the four cases.

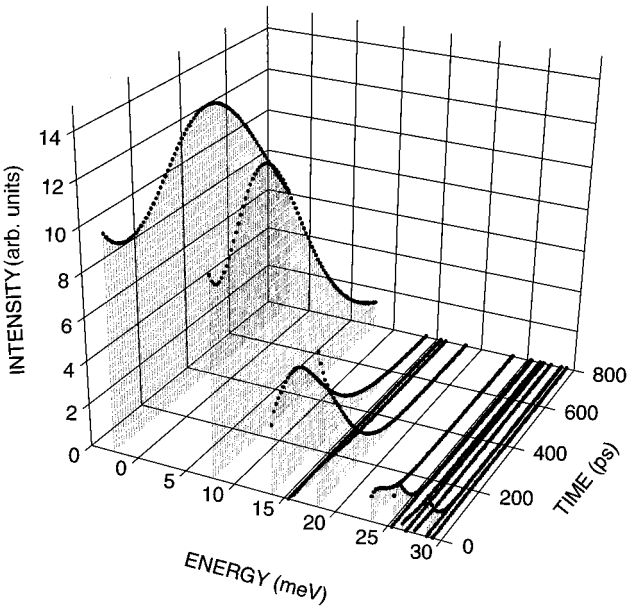

FIG. 3. Same as Fig. 1, without the Pauli exclusion principle.

Under the same excitation conditions the initial distribution is more degenerate for stronger lateral confinement. For $\hbar\omega_e = 6$ meV, we obtain a chemical potential $\mu = 24$ meV $\gg T_{\mathrm{ex}}$, while in the 2-meV case $\mu = 5.3$ meV is comparable to T_{ex}, which means a more classical energy distribution.

For the 6-meV dot with Pauli exclusion (Fig. 1), we observe a continuous time decay of the intensity. Comparing the integrated signal from the range 14–18 meV with the signal of the radiative lines at -2.6 and 7.8 meV, we can define three energy intervals of roughly equidistant spacing that exhibit a similar time dependence. The absence of an efficient population transfer between these energy intervals has two reasons: (1) The slowing down of LA phonon scattering renders direct scattering between the lowest radiative lines inefficient, as described in Sec. III B 1. (2) Relaxation through the intermediate nonradiative states is hindered by the Pauli principle since these states are widely occupied.

An internal dynamics is recovered for weaker lateral confinement (Fig. 2). In this case direct scattering between the radiative states is possible and the Pauli blocking of relaxation is less active due to the more classical carrier distribution (see above). There are characteristic plateaus in the time dependence of the low-energy lines. They arise from the combination of efficient relaxation and Pauli exclusion, which assures a population close to one for these states over a long time interval.

Assuming Bose statistics, the dynamics changes. For strong lateral confinement (Fig. 3), the signal from the interval 14–18 meV decreases much faster and the two lowest lines each acquire a pronounced maximum at sizable time delay. The fast decay is caused by relaxation through the closely spaced nonradiative levels (Fig. 3 of Ref. 22), which is possible although these states are occupied since there is no exclusion principle. Relaxation of excitons, the majority from nonradiative states, causes the delayed maxima for the two lowest lines.

For Bose statistics and weak lateral confinement (Fig. 4) the carriers relax very rapidly into the ground state, which

then acquires a population $n \gg 1$. The corresponding maximum intensity exceeds the values obtained in the former situations by about a factor of ten (compare the vertical scales of Figs. 1–4). The decay of this strong luminescence reflects the radiative lifetime of the ground state. In the other three cases, the time dependence is given by a complicated interplay of relaxation and recombination.

IV. EXPERIMENTAL TECHNIQUE

The experimental setup is schematically depicted in Fig. 5. Excitation is provided by a cw mode-locked Ti:sapphire laser pumped by an Ar^+ laser. 2-ps-duration pulses are used in the 685–720-nm range in order to excite resonantly the quantum dot structures. The repetition rate is 82 MHz. The pulse duration is systematically controlled by an autocorrelator. The excitation beam linearly polarized and adequately attenuated is focused through a microscope objective. The spot size at the sample surface is 1.5 μm (FWHM). The position and focusing of the exciting beam are controlled by a high precision xyz translation stage. The sample is mounted on a cold finger in a continuous-flow He cryostat, which allows measurements in the 5–100-K temperature range.

The photoluminescence signal from the sample, collected by the microscope objective, passes through a 200-μm pinhole located at an image plane. Thus, the observation is done on a restricted sample area (2–3 μm) and observation of a single dot is made possible. The signal is then dispersed by a 32-cm spectrometer with 300-g/mm gratings and detected by an optically triggered Hamamatsu streakscope. In this configuration the response time of the streakscope is 15 ps. The high stability of the excitation source allows a deconvolution procedure giving a slightly better time resolution. Thus, the overall spectral and time resolutions of the experimental setup are 2 meV and 10 ps. Part of the excitation beam is directly sent to the streakscope through a delay line in order to get a fixed time reference avoiding any jitter problems between two different data accumulations.

An analyzer is placed before the spectrometer to decrease the intensity of the scattered excitation light and to ensure a better signal-to-noise ratio for resonant excitation of the quantum dot. Nevertheless the minimum excess energy that we were able to achieve was only 18 meV. The mechanical stability of the setup allows integration times as long as 30 min without drifting away from the single dot.

V. EXPERIMENTAL RESULTS

In this section, we present the results of the time-resolved measurements. It is divided into four parts, according to the different physical dependencies that have been studied. In the first two parts, the dependence on the excitation wavelength (A) and excitation power (B) is discussed. This systematic variation of the excitation conditions provides us with information on the relaxation mechanism, active shortly after the excitation pulse and responsible for the rise of the PL. The time-dependent spectra at later times reflect the energy spectrum and the complex relaxation and recombination dynamics of the electron hole plasma. They show a characteristic dependence on the excitation power (B), the strength of the lateral confinement (C), and the sample temperature (D).

A. Excitation wavelength dependence

The depth of the lateral potential in the laser-induced quantum dots is about 35 meV, both for the electron and heavy hole. We have performed pulsed excitation with a photon energy between 18 and 66 meV above the lowest PL line. Thus this energy interval ranges from the case of resonant excitation deeply in the dot to resonant excitation close to the top of the confining lateral barrier. For an excess energy close to the LO phonon branch (36 meV in GaAs) resonant enhancement of relaxation by LO phonon emission into the ground state should occur. Below this LO phonon threshold remains relaxation by LA phonon scattering and, depending on the number of charge carriers, Coulomb scattering. For relaxation dominated by LO phonon emission, we would thus expect a sizable change when the excitation energy is scanned through $\hbar\omega_{\mathrm{LO}}$. This is not observed experimentally. As shown in Fig. 6, we always observe a fast rise of the ground-state PL, independently of the excitation wavelength. We see no resonant behavior at the excess energy of $\hbar\omega_{\mathrm{LO}}$. The rise time of about 10 ps, which is close to the time resolution of the experiment, is too short for relaxation by LA phonon scattering. These considerations indicate that Coulomb scattering, which can always promote part of the carrier distribution above $\hbar\omega_{\mathrm{LO}}$, and thus make LO phonon emission possible, is important. This result is further supported by the power dependence, to be presented in the next section. The fast rise of the PL and the absence of an effect at $\hbar\omega_{\mathrm{LO}}$ is observed for all excitation powers, all investigated quantum dot structures and for the whole temperature range.

B. Excitation power dependence

The excitation power determines the number of photoexcited electron-hole pairs in the dot. For excitation with picosecond pulses, we may safely neglect recombination during the pulse. The number of excitons in the dot, created by a single pulse, is estimated with the expression

$$N_{\mathrm{ex}} \cong \alpha\gamma\frac{P}{\nu\hbar\omega}. \tag{7}$$

An absorption probability of $\alpha = 6\times10^{-3}$ is used, a typical value for GaAs quantum wells. In the energy range where excitation is provided, the total level density in the quantum dot is sufficiently high to ensure that the absorption is not significantly different with respect to the unmodulated 2D case. The factor γ is the laser power that impinges onto the square dot of size w divided by the total power in the focused beam. The fraction on the right-hand side gives the number of photons per pulse. It is given by the measured average power P, the photon energy $\hbar\omega$, and the pulse repetition rate ν (82 MHz). For a Gaussian spot with 1.5 μm full width at half maximum, $P = 1\,\mu$W, $\hbar\omega = 1.7$ eV, and $w = 450$ nm, we thus obtain $N_{\mathrm{ex}} \cong 12.5$.

To describe the case of cw excitation, we define an average number N and a mean lifetime $\overline{\tau}$ of the excitons in the quantum dot. The relation

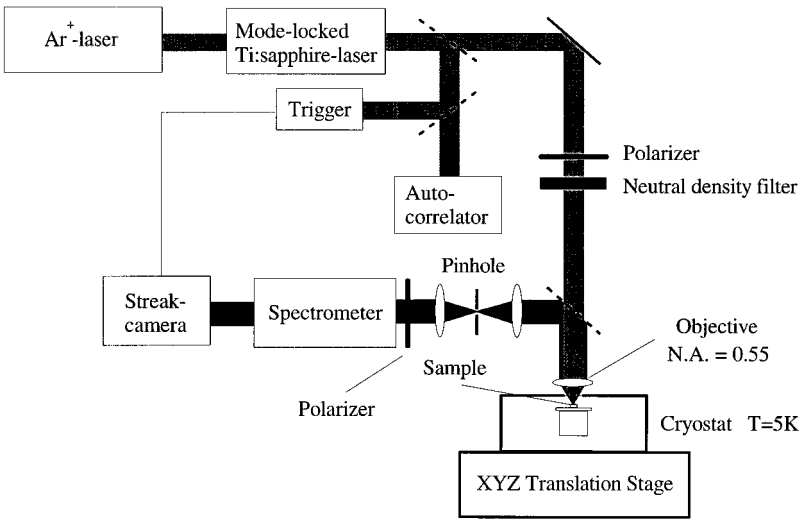

FIG. 5. Schematic diagram of the luminescence setup with temporal, spatial, and spectral resolution.

$$\alpha\gamma P=\hbar\overline{\omega}\frac{\overline{N}}{\overline{\tau}} \tag{8}$$

then describes the balance between the energy gain by photon absorption (left) and the energy loss by exciton recombination (right). From Eqs. (7) and (8) it follows that

$$\overline{N}=\alpha\gamma\frac{P\overline{\tau}}{\hbar\overline{\omega}}=N_{\mathrm{ex}}\overline{\tau}\nu\frac{\omega}{\overline{\omega}}. \tag{9}$$

Under the assumption that the relaxation is much faster than the recombination, which in quantum dots is not always justified (see Sec. III B 1), we can approximate $\overline{\tau}$ by the calculated lifetime. With $\hbar\overline{\omega}=1.96$ eV, $\overline{\tau}=10^{-10}$ s (Fig. 3 of Ref. 22) and $P=125$ nW, we thus estimate $N\cong 10^{-2}$ excitons for the μ-PL spectra of the 450-nm dot under weak cw excitation (Fig. 4 of Ref. 12). The cw estimation has to be considered with some precaution because there could be an accumulation of charge carriers in states that are weakly coupled to the light; this would mean a longer effective lifetime $\overline{\tau}$ and therefore a higher exciton number N. This problem does not exist for pulsed excitation as long as the time interval ν^{-1} between the individual pulses is long enough to ensure that all photoexcited carriers recombine before the next pulse arrives.

We have employed laser powers between 140 nW and 14 μW. According to the above estimate, this corresponds to the range from 1–2 to 170 excitons in the dot. In Fig. 7, we present the measured temporal change of the PL spectrum for three different laser powers. Within about the first 100 ps, the spectra appear broadened to an amount that increases with increasing excitation power. This density-dependent broadening strongly supports the interpretation that Coulomb scattering contributes significantly to the initial stage of energy relaxation.

With increasing time delay, the broadening decreases and the late spectra consist of a number of distinct peaks. The relative intensity of the peaks changes systematically with laser power. This dependence is shown more clearly in Fig. 2 of Ref. 22, where a series of spectra measured with different laser power are directly superimposed. The spectra are recorded without intentionally changing the lateral position and the focus of the laser spot on the sample. In fact it is important to avoid lateral drift of the sample during the long accumulation time of the measurements, since we have observed that the relative intensities of the lines can change in a nonsymmetric way when the sample is intentionally dis-

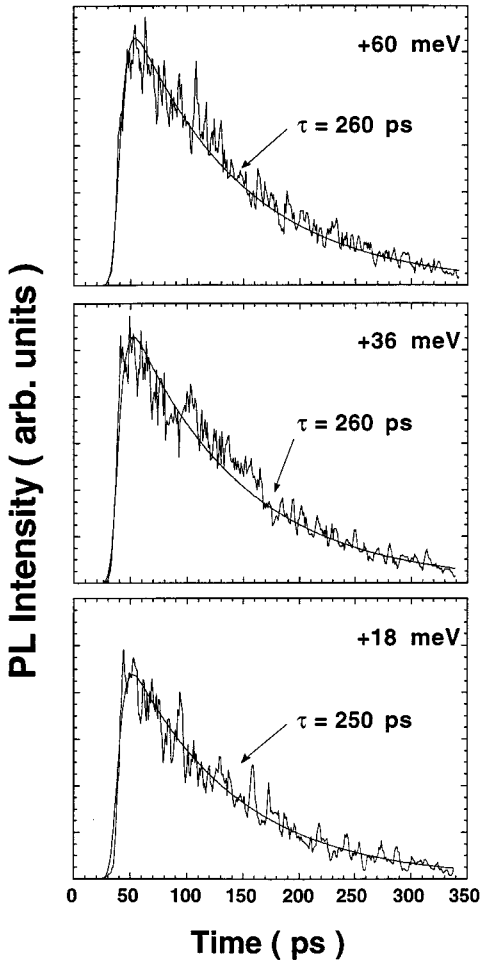

FIG. 6. Time dependence of the fundamental transition of the $w=450$ nm quantum dot for three excitation energies above and below the LO phonon emission threshold. $P=4.5$ μW, $T_l=7$ K.

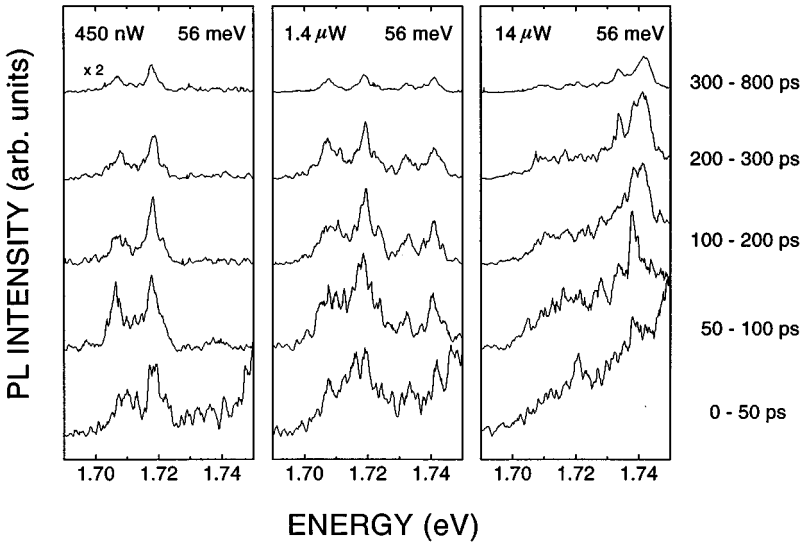

FIG. 7. Photoluminescence spectra of the single dot $w=450$ nm for different time delay windows. The excitation power P increases from left to right, as indicated at the top of each figure. Pulsed excitation is provided at 1.764 eV, 59 meV above the lowest luminescence line. The sample temperature is 7 K.

placed with respect to the microscope objective. Such a displacement decentralizes both the excitation and the detection on the dot. We have carefully checked the power dependence presented in Fig. 2 of Ref. 22 with a second series of measurements where the position of the laser spot has been recentralized for each spectrum. For an excitation power of 450 nW, two main peaks separated by about 10 meV are observed. Taking into account the smaller spectral resolution in the time-resolved measurement, this spectrum is very similar to the one observed under weak cw excitation. With increasing power of the resonant excitation, two additional strong lines appear and the spectral weight shifts systematically to higher energy. Only under resonant, pulsed excitation are we able to observe the two strong higher-energy transitions. In the cw case, an increase in laser power from 125 nW to 20 μW causes a considerable broadening but the two high-energy lines only appear as weak structures.[12]

The observed strong power dependence is attributed to a successive filling of excited states. The almost equidistant spacing of all 4 lines compares well with the calculation for $\hbar\omega_e=6$ meV. If Fermi statistics is assumed, the theoretical shift of the Fermi energy by about 30 meV (left part of Fig. 3 of Ref. 22) is consistent with the appearance of the two higher-energy lines in the experimental spectra. With increasing power (i.e., exciton number) the lowest states first acquire a sizable occupation. The level degeneracy is higher at the excited-state energies. As a consequence, the lowest peaks saturate at intermediate power levels, while the upper ones increase with P up to 14 μW.

Let us now consider the dependence of the peak positions on the excitation power, i.e., the estimated exciton number N_{ex}. The two lowest lines shift by about 1 meV to lower energy with N_{ex} increasing from about 1 to 60. The position of the two higher-energy levels appears to be independent of N_{ex} within the experimental accuracy. The very weak energy shifts indicate that the spectrum remains of excitonic origin. For cw excitation the estimated exciton number in the dot is about 10^{-2} and the emission spectrum is excitonic. Increasing the exciton number in the dot up to about 1 with cw excitation[12] and to about 200 with pulsed excitation, only a very small shift of the emission spectrum occurs. Therefore we conclude that the spectrum remains of excitonic origin. The PL spectrum of the photoexcited electron-hole plasma can be interpreted in terms of an exciton gas over the whole range of N_{ex}. The state filling effect indicates Fermi statistics.

C. Dependence on the lateral confinement

Up to this point we have presented results on the quantum dot structure of $w=450$ nm. This structure exhibits by far the strongest lateral confinement within the investigated series of quantum dots fabricated by laser-induced thermal intermixing of one quantum well. We have also studied dots with geometrical sizes of 400, 500, 600, and 1000 nm. All these structures of weak lateral confinement exhibit the same qualitative behavior in the time-resolved measurements. In this section, we show, taking the example of the 500-nm dot, that this behavior strongly differs from the one observed for strong lateral confinement. On the 500-nm dot a PL line splitting of about 4 meV is observed (Fig. 1 of Ref. 12), which in the theoretical description corresponds to $\hbar\omega_e=2$ meV. Due to the smaller lateral confinement, the individual lines are not resolved in the time-resolved spectra shown in Fig. 2 of Ref. 22. Again we observe a blueshift of the spectral weight with increasing laser power. Due to the higher density of states, this blueshift is, however, much smaller than in the $w=450$ nm dot. The experimentally observed blueshifts of different size are in agreement with the theoretical results obtained for $\hbar\omega_e=2$ meV and 6 meV (top of Fig. 3 of Ref. 22).

In Fig. 4 of Ref. 22, we compare the time dependence of the PL of the weak and the strong confinement case. The same nominal excitation conditions are used. For weak lateral confinement, a transfer of intensity from the higher-to the lower-energy part of the PL spectrum is detected with increasing time. The spectral weight of the PL shifts systematically to the ground state, as exemplified by the time evolution of the selected spectral windows in the right side of the figure. The decay times, obtained from a fit to the temporal decay of the PL, decrease with increasing energy. On the strong confinement sample, the $w=450$ nm dot, a strikingly different recombination dynamics is observed. The excited-state transitions exhibit comparable or even longer

decay times than the ground state. No systematic transfer of intensity from higher to lower energy is observed on this quantum dot. The observed dynamics resembles our theoretical results for an exciton gas with Fermi statistics presented in Fig. 1 for strong and in Fig. 2 for weak lateral confinement. Notice the plateaulike time dependence at short time delay observed for $w=500$ nm. Theory predicts such an effect (Fig. 2), however in a more pronounced form than experimentally observed.

On the other hand, the experimental results are fully inconsistent with the assumption of an exciton gas with Bose statistics (Figs. 3 and 4). None of the two striking qualitative features of the dynamics in the Bose case is experimentally observed. For strong lateral confinement ($w=450$ nm, corresponding to Fig. 3), the lowest PL maximum should appear more than 400 ps after the pulse; the measured value is below 50 ps. We also do not observe the one order of magnitude difference in the peak intensity of the lowest PL line between the 450- and 500-nm quantum dot structure, to be expected from the comparison of Figs. 3 and 4.

D. Temperature dependence

Raising the sample temperature from 5 K up to 60 K, a qualitatively different behavior is observed for the quantum dot series and the reference quantum well (Fig. 8). In the temperature range (5–25 K) where the PL intensities (upper part) are essentially constant the PL recombination time (lower part) increases for the quantum well but decreases slightly for the dots. The increase of the quantum-well decay time is a typical result obtained when excitation is performed with a nonzero excess energy. It is attributed to the thermal excitation of excitons or polaritons from radiative states at the bottom of the 2D subband to nonzero center-of-mass momentum states, which are not coupled to the light.[40–42] In the μ-PL arrangement the measured quantum-well decay time can be affected by spatial diffusion of the carriers out of the detection range. Recent measurements of the exciton in-plane diffusion constant indicate that the 60-K decay time could be influenced by this effect, while at lower temperature the diffusion length should be small compared to the spot size.[43]

In a quantum dot the translational invariance is broken, which leads to higher-energy radiative states. Therefore the thermal depopulation of the lowest states does not necessarily imply an increase in the decay time in contrast to the case of a quantum well. Considering the decay of a single isolated 0D state we would expect a negligible temperature dependence. In practice, the temporal decay of the quantum dot lines will vary according to the temperature dependence of the energy relaxation, of the carrier distribution and of the nonradiative decay rates. We observe a systematic decrease of the decay time of the spectrally integrated PL with increasing temperature and with decreasing geometrical size w (Fig. 8). This is attributed to the activation of nonradiative loss mechanisms, which might be related to structural defects in the intermixed barriers. We cannot explain the complex temperature dependence by simply considering thermal activation out of the dot above the lateral barrier. An exponential activation law with an activation energy given by the energy difference between the 0D state and the top of the lateral barrier does not well describe the measured results.

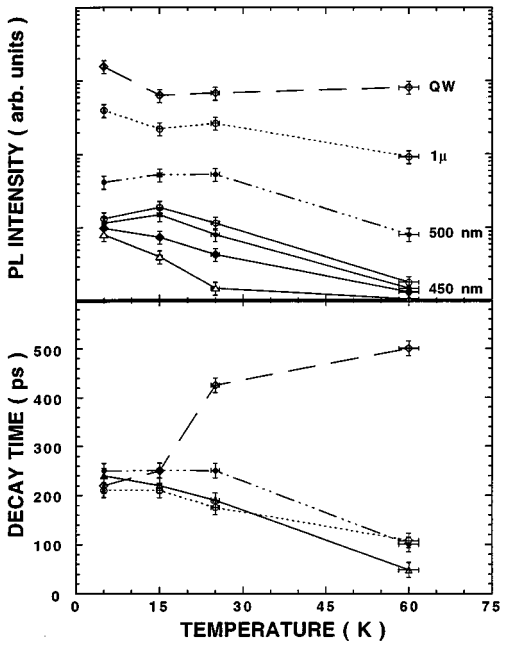

FIG. 8. Temperature dependence of the intensity (top) and the decay time (bottom) of the spectrally integrated PL for single quantum dot structures of various geometrical size w and the as-grown quantum well (dashed line ◇: quantum well; dotted line ○: $w=1\mu$m; dashed-dotted line with ●: 500 nm; solid line, 450 nm; ground (●), first excited (○), second excited (◆), and third excited (△) state). Apart from the PL intensity for 450 nm all experimental points correspond to an average over the PL spectrum. The horizontal error bars give the temperature variation during the measurement, detected by a temperature sensor located close to the sample. Pulsed excitation is provided at 1.764 eV with an average power P of 2.5 μW.

The temperature-induced change within the PL spectrum of the $w=450$ nm quantum dot is presented in Fig. 9. With increasing temperature the relaxation becomes faster for two reasons: (i) the exciton-LA phonon scattering rates increase, (ii) the more classical exciton distribution leads to a less efficient Pauli blocking of the relaxation. This gives rise to an accelerated decay of the excited states, in qualitative accordance with the decrease in the relative intensity of the higher-energy lines with temperature of 5, 15 and 25 K. Quantitatively, however, using the theoretical model described above, we expect a smaller temperature effect than is experimentally observed. We therefore attribute part of the decrease in high-energy intensity to a systematic decrease of the number of carriers in the dot with increasing temperature, in accordance with the above-mentioned influence of nonradiative recombination and escape mechanisms. That the relaxation dynamics effectively changes with temperature is clearly seen from Fig. 10. At higher temperature a systematic decrease of the decay time with increasing energy is recovered, the qualitative difference between the dynamics of the strong and weak confinement case diminishes.

VI. CONCLUSIONS

The observation of up to four almost equidistantly spaced PL peaks suggests that the *shape of the lateral confinement*

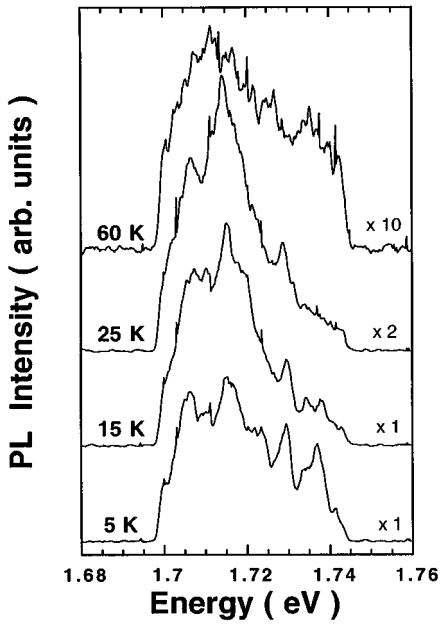

FIG. 9. Time-integrated spectra of the $w=450$ nm quantum dot at different temperatures. The relatively strong broadening is caused by the integration over the full time interval (0–800 ps), which notably includes the initial stage of relaxation (compare Fig. 7, 0-100 ps). The full time interval is used to systematically compare the spectra up to the maximum temperature of 60 K where the photoexcited carriers recombine to a large extent already within 200 ps after the pulse. $P=2.5\mu$W.

potential of the investigated quantum dot structures is essentially parabolic. Nevertheless, deviations from a perfectly symmetric shape should exist. This follows from a number of observations on the $w=450$ nm structure: (i) the first excited state exhibits a fine structure, which is well resolved in the low-power cw spectrum, (ii) the intensity of the two high-energy lines compared to the two low-energy lines depends in a nonsymmetric way on the position of the sample with respect to the point of local excitation and detection, (iii) more radiative lines appear in the spectra than are theoretically expected for a parabolic lateral potential with rotational symmetry, (iv) nonradiative processes seem to become important at rather low temperature. It remains that within our series of quantum dots each structure exhibits a discrete, individual energy spectrum. The strength of the spatial quantization is varied and pronounced 0D effects are systematically observed on the sample with strongest lateral confinement, the $w=450$ nm dot. It would be interesting to perform similar time-resolved studies also on other types of quantum dot structures. For instance, the confining potentials of epitaxially grown quantum dots are expected to be nonparabolic and stronger than in the present case.

We find several experimental indications for an *important contribution of Coulomb scattering to the process of energy relaxation.* First, there is the density-dependent broadening of the spectra at short time delays, which increases with the excitation power. Second, a fast rise of the PL is observed independently of the lateral confinement and the sample temperature. Third, we observe no pronounced effects when the excitation wavelength is varied through the threshold for LO phonon emission. The measurements indicate that relaxation by means of Auger processes[28] is efficient down to very low excitation power. This might also explain the efficient luminescence and the short PL rise time observed on epitaxially grown $InAs/In_xGa_{1-x}As$ quantum dot island structures.[13,33,34,44,45] It would be interesting to improve the time resolution and to measure the dependence of the PL rise time on the number of photoexcited carriers. This could provide additional information on the relative importance of

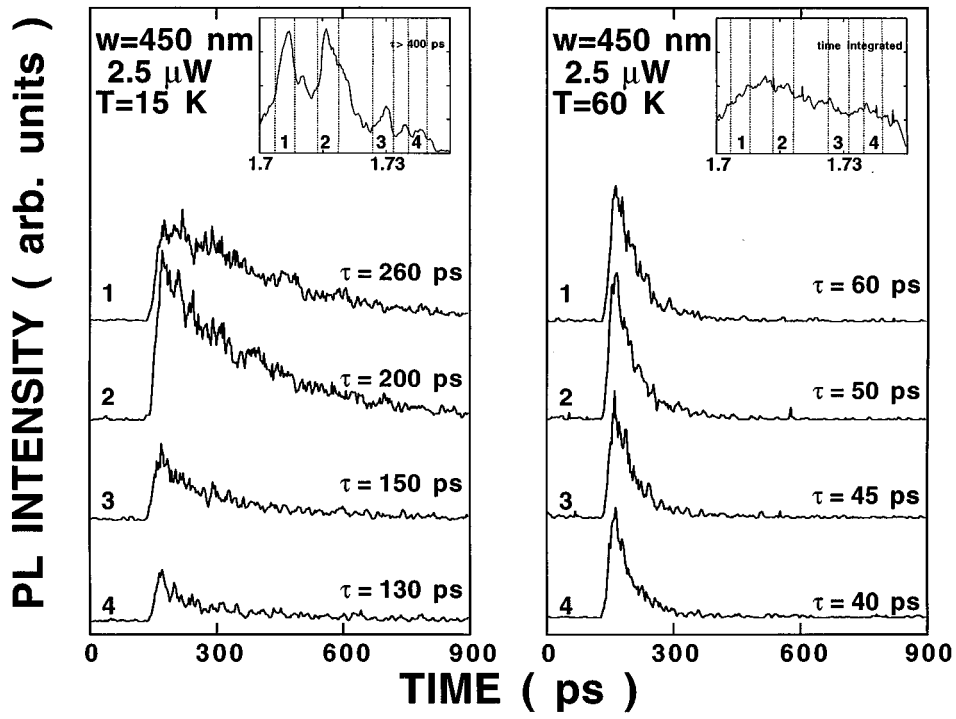

FIG. 10. Time dependence of the PL intensity from selected spectral windows for the $w=450$ nm quantum dot, at 15 K (left) and 70 K (right). The spectrum given in the inset is integrated over times of more than 400 ps after the excitation pulse for $T=15$ K and from 0 to 800 ps for $T=60$ K.

carrier-carrier and carrier-phonon scattering in the energy relaxation.

Strikingly different behavior is observed for the sample with the strongest confinement as compared to all the other structures of our series. The strong confinement sample shows pronounced 0D effects. Increasing the number of excitons in the dot from about 1–2 to 200, additional excited-state transitions appear up to more than 30 meV above the ground state. This extremely strong variation of the spectrum demonstrates the small density of states caused by the complete spatial quantization. It is accompanied by a surprisingly weak shift of the discrete lines. These small shifts and the similarity between the low-power time-resolved and the cw spectra strongly suggest an excitonic description over the entire range of excitation power. The calculated behavior of a *Fermi gas of excitons in a quantum dot* is in qualitative agreement with our experimental findings: (i) state filling is observed in the spectrum with increasing laser power, (ii) in the strong confinement sample at low temperature we see no population transfer from higher to lower energy with increasing time, (iii) an internal relaxation dynamics is recovered by decreasing the strength of the lateral confinement.

By the present work we have demonstrated that PL spectroscopy of a single quantum dot is possible with picosecond time resolution. Using resonant excitation and low excitation power we have been able to avoid sizable heating, as is evidenced by the narrow linewidths. The sensitivity of the experiment is excellent, the ultimate limit of a single exciton per pulse in the dot has been approached. We believe that time-resolved μ-PL spectroscopy has the potential to become an important technique in the field of semiconductor nanostructures.

ACKNOWLEDGMENTS

We thank K. Brunner, G. Böhm, and G. Weimann for providing the samples and G. Abstreiter, G. Bastard, C. Delalande, J. Y. Marzin, B. Ohnesorge, P. Voisin, and M. Voos for support or helpful suggestions. The work has been supported financially by the Deutsche Forschungsgemeinschaft (SFB 348) and a PROCOPE contract. One of us (A.F.) is grateful for a Human Capital and Mobility grant of the European Community (ERBCHBICT 930654).

[1] Ch. Sikorski and U. Merkt, Phys. Rev. Lett **62**, 2164 (1989).
[2] H. Drexler, D. Leonard, W. Hansen, J. P. Kotthaus and P. M. Petroff, Phys. Rev. Lett. **73**, 2252 (1994).
[3] M. A. Reed, J. N. Randall, R. J. Aggarwal, R. J. Matyi, T. M. Moore, and A. E. Wetsel, Phys. Rev. Lett. **60**, 535 (1988).
[4] P. L. McEuen, E. B. Foxman, U. Meirav, M. A. Kastner, Y. Meir, N. S. Wingreen, and S. J. Wind, Phys. Rev. Lett. **66**, 1926 (1991).
[5] A. T. Johnson, L. P. Kouwenhoven, W. de Jong, N. C. van der Vaart, C. J. P. M. Harmans, and C. T. Foxon, Phys. Rev. Lett. **69**, 1592 (1992).
[6] W. Hansen, T. P. Smith, K. Y. Lee, J. A. Brum, C. M. Knoedler, J. M. Hong, and D. P. Kern, Phys. Rev. Lett. **62**, 2168 (1989).
[7] R. C. Ashoori, H. L. Stormer, J. S. Weiner, L. N. Pfeiffer, K. W. Baldwin, and K. W. West, Phys. Rev. Lett. **71**, 613 (1993).
[8] R. Strenz, U. Bockelmann, F. Hirler, G. Abstreiter, G. Böhm, and G. Weimann, Phys. Rev. Lett. **73**, 3022 (1994).
[9] L. Brey, N. Johnson, and B. I. Halperin, Phys. Rev. B **40**, 10 647 (1989).
[10] K. Karraï, X. Ying, H. D. Drew, and M. Shayegan, Phys. Rev. B **40**, 12 020 (1989).
[11] J. Y. Marzin, A. Izraël, J. Y. Parzin, R. Azoulay, V. Thierry-Mieg, and F. R. Ladan, Appl. Phys. Lett. **61**, 3023 (1992).
[12] K. Brunner, U. Bockelmann, G. Abstreiter, M. Walther, G. Böhm, G. Tränkle, and G. Weimann, Phys. Rev. Lett. **69**, 3216 (1992).
[13] J.-Y. Marzin, J.-M. Gérard, A. Izraël, D. Barrier, and G. Bastard, Phys. Rev. Lett. **73**, 716 (1994).
[14] K. Brunner, G. Abstreiter, G. Böhm, G. Tränkle, and G. Weimann, Appl. Phys. Lett. **64**, 3320 (1994).
[15] A. Zrenner, L. V. Butov, M. Hagn, G. Abstreiter, G. Böhm, and G. Weimann, Phys. Rev. Lett. **72**, 3382 (1994).
[16] K. Brunner, G. Abstreiter, G. Böhm, G. Tränkle, and G. Weimann, Phys. Rev. Lett. **73**, 1138 (1994).
[17] D. Gammon, E. S. Snow, B. V. Shanabrook, D. S. Katzer, and D. Park, Phys. Rev. Lett. **76**, 3005 (1996).
[18] H. F. Hess, E. Betzig, T. D. Harris, L. N. Pfeiffer, and K. W. West, Science **264**, 1740 (1994).
[19] L. Novotny and D. W. Pohl, in *Photons and Local Probes*, edited by O. Marti and R. Möller, Vol. 300 of *NATO Advanced Studies Institute Series E: Physics* (Kluwer Academics, Dordrecht, 1995), p. 21.
[20] L. Novotny, D. W. Pohl, and B. Hecht, Opt. Lett. **20**, 972 (1995).
[21] M. Grundmann, J. Christen, N. N. Ledentsov, J. Böhrer, D. Bimberg, S. S. Ruvimov, P. Werner, U. Richter, U. Gösele, J. Heydenreich, V. M. Ustinov, A. Yu. Egorov, A. E. Zhukov, P. S. Kop'ev, and Zh. I. Alferov, Phys. Rev. Lett. **74**, 4043 (1995).
[22] U. Bockelmann, Ph. Roussignol, A. Filoramo, W. Heller, G. Abstreiter, K. Brunner, G. Böhm, and G. Weimann, Phys. Rev. Lett. **76**, 3622 (1996).
[23] U. Bockelmann, Ph. Roussignol, A. Filoramo, W. Heller, and G. Abstreiter, Solid State Electron. **40**, 541 (1996).
[24] U. Bockelmann, W. Heller, and G. Abstreiter, following paper, Phys. Rev. B **58**, 4469 (1997).
[25] U. Bockelmann and G. Bastard, Phys. Rev. B **42**, 8947 (1990).
[26] H. Benisty, C. M. Sotomayor Torres, and C. Weisbuch, Phys. Rev. B **44**, 10945 (1991).
[27] T. Inoshita and H. Sakaki, Phys. Rev. B **46**, 7260 (1992).
[28] U. Bockelmann and T. Egeler, Phys. Rev. B **46**, 15 574 (1992).
[29] K. Brunner, U. Bockelmann, G. Abstreiter, M. Walther, G. Böhm, G. Tränkle, and G. Weimann, J. Phys. (France) IV **3**, 107 (1993).
[30] U. Bockelmann, K. Brunner, and G. Abstreiter, Solid State Electron. **37**, 1109 (1994).
[31] D. A. Broido, A. Cros, and U. Rössler, Phys. Rev. B **45**, 11 395 (1992).
[32] T. Darnhofer, D. A. Broido, and U. Rössler, Phys. Rev. B **50**, 15 412 (1994).
[33] G. Wang, S. Fafard, D. Leonhard, J. E. Bowers, J. L. Merz, and P.

M. Petroff, Appl. Phys. Lett. **64**, 2815 (1994).
[34] R. Nötzel, J. Temmo, and T. Tamamura, Nature **369**, 131 (1994).
[35] Ph. Lelong and G. Bastard, Solid State Commun. **98**, 819 (1996).
[36] U. Bockelmann, Phys. Rev. B **48**, 17 637 (1993).
[37] Y. Z. Hu, S. W. Koch, M. Lindberg, N. Peyghambarian, E. L. Pollock, and Farid F. Abraham, Phys. Rev. Lett. **64**, 1805 (1990).
[38] A. Barenco and M. A. Dupertuis, Phys. Rev. B **52**, 2766 (1995).
[39] U. Bockelmann, Phys. Rev. B **50**, 17 271 (1994).
[40] J. Feldmann, G. Peter, E.O. Göbel, P. Dawson, K. Moore, C. Foxon, and R. J. Elliott, Phys. Rev. Lett. **59**, 2337 (1987).
[41] L. C. Andreani, F. Tassone, and F. Bassani, Solid State Commun. **77**, 61 (1991).
[42] D. S. Citrin, Phys. Rev. Lett. **69**, 3393 (1992).
[43] A. Filoramo, W. Heller, Ph. Roussignol, and U. Bockelmann (unpublished).
[44] J. M. Gérard, in *Confined Electrons and Photons: New Physics and Devices*, edited by C. Weisbuch and E. Burstein, Vol. 340 of *NATO Advanced Studies Institute Series B: Physics* (Plenum, New York, 1995), p. 357.
[45] S. Grosse, J. H. H. Sandmann, J. Feldmann, H. Lipsanen, M. Sopanen, J. Tulkki, and J. Ahopelto, Phys. Rev. B (to be published).